Electron Bernstein wave emission based diagnostic on National Spherical Torus Experiment (invited)[a]

S. J. Diem,[1] G. Taylor,[1] J. B. Caughman,[2] P. Efthimion,[1] H. Kugel,[1] B. P. LeBlanc,[1]
J. Preinhaelter,[3] S. A. Sabbagh,[4] J. Urban,[3] and J. Wilgen[2]

[1]*Princeton Plasma Physics Laboratory, P.O. Box 451, Princeton, New Jersey 08543, USA*
[2]*Fusion Energy Division, Oak Ridge National Laboratory, P.O. Box 2008, Oak Ridge, Tennessee 37831-6169, USA*
[3]*EURATOM/IPP.CR Association, Institute of Plasma Physics, 18200 Prague 8, Czech Republic*
[4]*Department of Applied Physics and Applied Mathematics, Columbia University, New York 10027, USA*

National Spherical Torus Experiment (NSTX) is a spherical tokamak (ST) that operates with n_e up to 10^{20} m^{-3} and B_T less than 0.6 T, cutting off low harmonic electron cyclotron (EC) emission widely used for T_e measurements on conventional aspect ratio tokamaks. The electron Bernstein wave (EBW) can propagate in ST plasmas and is emitted at EC harmonics. These properties suggest thermal EBW emission (EBE) may be used for local T_e measurements in the ST. Practically, a robust $T_e(R,t)$ EBE diagnostic requires EBW transmission efficiencies of $>90\%$ for a wide range of plasma conditions. EBW emission and coupling physics were studied on NSTX with an obliquely viewing EBW to O-mode (B-X-O) diagnostic with two remotely steered antennas, coupled to absolutely calibrated radiometers. While $T_e(R,t)$ measurements with EBW emission on NSTX were possible, they were challenged by several issues. Rapid fluctuations in edge n_e scale length resulted in $>20\%$ changes in the low harmonic B-X-O transmission efficiency. Also, B-X-O transmission efficiency during H modes was observed to decay by a factor of 5–10 to less than a few percent. The B-X-O transmission behavior during H modes was reproduced by EBE simulations that predict that EBW collisional damping can significantly reduce emission when $T_e < 30$ eV inside the B-X-O mode conversion (MC) layer. Initial edge lithium conditioning experiments during H modes have shown that evaporated lithium can increase T_e inside the B-X-O MC layer, significantly increasing B-X-O transmission. © *2008 American Institute of Physics.* [DOI: 10.1063/1.2953592]

I. INTRODUCTION

Spherical tokamaks (STs) routinely operate with plasmas that have high electron densities, n_e, and low toroidal magnetic fields, B_T, such that the plasmas are overdense, $\omega_{pe} \gg \Omega_{ce}$, where ω_{pe} is the electron plasma frequency and Ω_{ce} is the electron cyclotron (EC) frequency. Traditionally, tokamaks and many other magnetically confined plasmas devices have utilized EC waves to provide local electron temperature, T_e, measurements via EC emission (ECE).[1] In these overdense devices, the propagation of low harmonic EC waves beyond the plasma edge is cutoff, prohibiting the use of ECE for T_e measurements. The National Spherical Torus Experiment[2] (NSTX) routinely studies plasma in the overdense regime, with n_e up to 10^{20} m^{-3} and $B_t < 0.6$ T, so that ECE at the first five EC harmonics is cut off. An alternative to EC waves in this overdense regime is the electrostatic electron Bernstein wave (EBW),[3] which propagates mainly perpendicular to the external magnetic field and is strongly emitted near EC harmonics. Unlike electromagnetic EC waves, EBWs do not experience a density cutoff in the plasma. The EBW cannot propagate in vacuum, but must couple to an ordinary (O) or extraordinary (X) electromagnetic wave in order to be detected by a receiving antenna located outside of the vacuum vessel. Coupling to the EBW can be achieved through two mode conversion (MC) schemes: B-X (EBW to X-mode coupling) (Ref. 4) and the double MC process of B-X-O (EBW to X-mode to O-mode coupling) MC.[5] Currently, NSTX is studying thermal emission via B-X-O MC. In this conversion process thermal EBW emission (EBE), generated near an EC harmonic resonance, travels toward the plasma edge until it mode converts to the slow X mode at the upper hybrid resonance (UHR) layer where $\omega = [(\omega_{pe})^2 + (\Omega_{ce})^2]^{1/2}$. At the UHR layer, the perpendicular wave vector, $k\perp$, of the EBW and the slow X-mode branch are equal and full conversion between the two branches occurs. The slow X mode propagates back into the plasma until it encounters the left-hand cutoff of the X mode (where $\omega = (1/2)[-\Omega_{ce} + (\Omega_{ce}^2 + 4\omega_{pe}^2)^{1/2}]$). For particular oblique viewing angles, the left-hand cutoff of the slow X-mode branch is coincident with the O-mode cutoff (where $\omega = \omega_{pe}$) and the power in the slow X mode is transferred to the O-mode branch. The B-X-O MC efficiency is given by[6,7]

$$T(n_\perp, n_\parallel) = \exp(-\pi k_0 L_n \sqrt{(Y/2)}[2(1+Y)(n_{\parallel,opt} - n_\parallel)^2 + n_\perp^2]), \tag{1a}$$

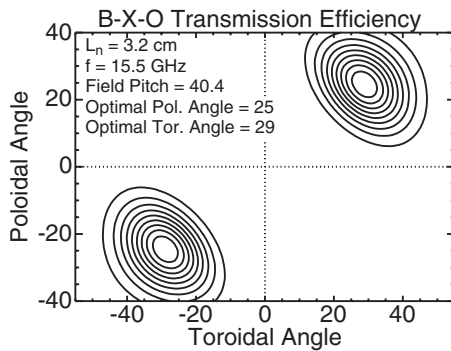$$n_{\parallel,opt}^2 = \left(\frac{Y}{Y+1}\right) = \cos^2(\phi_{opt}), \tag{1b}$$

FIG. 1. *B-X-O* MC efficiency map, Eq. (1a), is shown as a function of toroidal and poloidal angle for 15.5 GHz fundamental emission from an *L*-mode plasma. The center contour represents the angular region where >90% transmission occurs. Each contour thereafter represents a 10% decrease in the MC efficiency.

$$Y = \left(\frac{\Omega_{ce}}{\omega} \right). \tag{1c}$$

In the equations above, $n_\parallel$ and $n\perp$ are the parallel and perpendicular indices of refraction, respectively, and L_n is the density scale length evaluated at the UHR. An example of the calculated *B-X-O* MC efficiency window for a NSTX plasma is shown in Fig. 1. Two angular emission windows are available for a given frequency: one along the magnetic field (positive angles) and the other against the magnetic field (negative angles). The center of the *B-X-O* transmission window in poloidal and toroidal angle depends on the magnetic field and the magnetic field pitch at the MC layer. L_n at the MC layer determines the angular width of the window. By decreasing L_n, the angular width of the window is increased. The *B-X-O* MC efficiency in Eq. (1a) only calculates the MC at the *O*-mode cutoff layer and does not account for re-absorption and re-emission prior to *B-X-O* conversion. An EBE simulation code was used to calculate these losses.

This paper presents details of EBE measurements made via *B-X-O* MC on NSTX and discusses the challenges for reconstructing $T_e(R)$ from these measurements. Section II describes the *B-X-O* emission diagnostic used on NSTX and the EBE simulation code used to interpret the emission measurements. Section III A presents results that show the effect of density fluctuations on the *B-X-O* transmission, Sec. III B presents results that show the effect of EBW collisional damping, and in Sec. III C a $T_e(R)$ profile is reconstructed from the emission. The implications of the results are discussed in Sec. IV.

II. EBE DIAGNOSTIC AND SIMULATION CODE

EBE measurements on NSTX are acquired with two remotely steered, quadridged microwave antennas measuring fundamental, second and third harmonic emissions in the frequency range of 8–36 GHz.[8] The antennas are mounted outside of the vacuum vessel, 50 cm from the plasma edge. The antenna ridges are oriented to measure emission polarization components perpendicular and parallel to the magnetic field at the MC layer. The total radiation temperature, T_{rad}, is determined by adding the two polarization components to-

gether. Each antenna mount has two linear actuators to control movement in the poloidal and toroidal directions, allowing a scan of the *B-X-O* transmission window. The antennas are each coupled to a dual-channel heterodyne radiometer, one measuring 8–18 GHz and the other 18–36 GHz emission. This paper will only present emission results from the 18–36 GHz radiometer range. A quadridged microwave horn antenna (Q-par Angus Ltd., model No. WBH18-40DPK) with a broadband frequency coverage of 18–40 GHz was coupled to the 18–36 GHz radiometer utilizing a Miteq SBE0440 LW1 second harmonic mixer (Fig. 2). The noise temperature of the radiometer is 0.5–1 eV. A relatively narrow bandwidth of 175 MHz was chosen because in high β ST plasmas there is very little change in the EBE frequency between the axis and the last closed flux surface (LCFS). The average effective resolution with an intermediate frequency bandwidth of 175 MHz is about 2–3 cm. The frequency coverage is achieved via two separate voltage-controlled oscillators (VCOs): one with a range of 8–12 GHz and the second with a range of 12–18 GHz. The two VCOs are alternately activated via a TTL logic controlled switch (American Microwave Corp. SPDT 8–18 GHz switch, shown in Fig. 3). The VCOs are frequency scanned at 10 kHz, via an Agilent 33120A waveform generator, to measure the evolution of the emission spectrum.

The radiometers are absolutely calibrated using the Dicke switching method.[9] For this method, the antenna switches at a rate of 40 Hz between looking at a room temperature blackbody source ($T = 300$ K) and a liquid nitrogen temperature blackbody source ($T = 77$ K). The antenna signal is sent to the radiometer tuned to a particular frequency. The voltage output from the radiometer is proportional to the radiation temperature of the emission given by: $V_{out} = G(f)*T_{rad}$, where $G(f)$ is the frequency-dependent gain factor (V/eV) and is given by the ratio of the change in voltage divided by the change in temperature, $\Delta V/\Delta T$. For this calibration process, $\Delta T = 300 - 70$ K. The change in radiometer voltage, ΔV, is extremely small so a lock-in amplifier is used during the calibration. A 2.5 s integration time constant provided an output signal averaged over more than 100 Dicke switching cycles. The absolute calibration included the microwave cables, radiometer quadridged antenna, and vacuum window used for measuring plasma emission during NSTX experiments.

The optical depth for EBWs at low harmonic EC resonances is ~3000 in NSTX, well satisfying the blackbody condition, so the measured T_{rad} can be assumed to be equal to the local T_e, provided the *B-X-O* MC efficiency is ~100%. For cases where the *B-X-O* MC efficiency is not equal to 100%, EBE simulations were used to deduce T_e.

The emission measurements were simulated with an EBE numerical code developed by Preinhaelter *et al.*[10] The code simulates the process of *O-X-B* injection; however, due to the reciprocity of the injection and emission processes,[11] the absorption and emission locations are the same. A bundle of 41 rays are launched in the code to simulate the antenna pattern of the EBE diagnostic. A full-wave code[12] calculates the MC efficiency of the *O-X-B* MC assuming a one dimen-
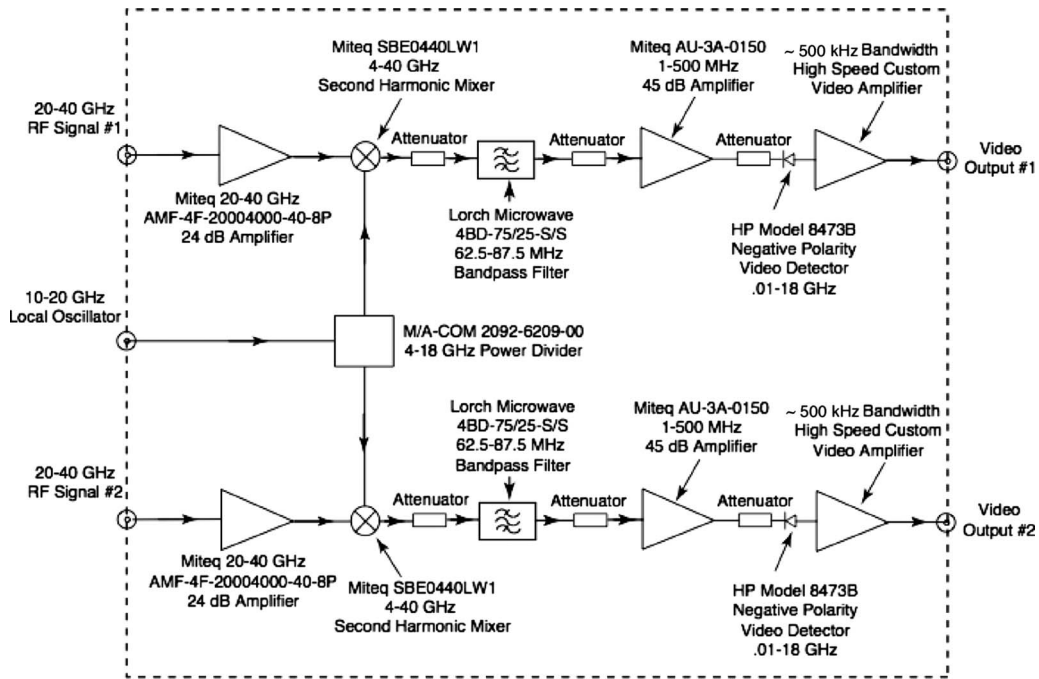
NSTX Dual-Channel 20-40 GHz EBW Radiometer

FIG. 2. Shown is a schematic of the 18–36 GHz dual-channel heterodyne radiometer system.
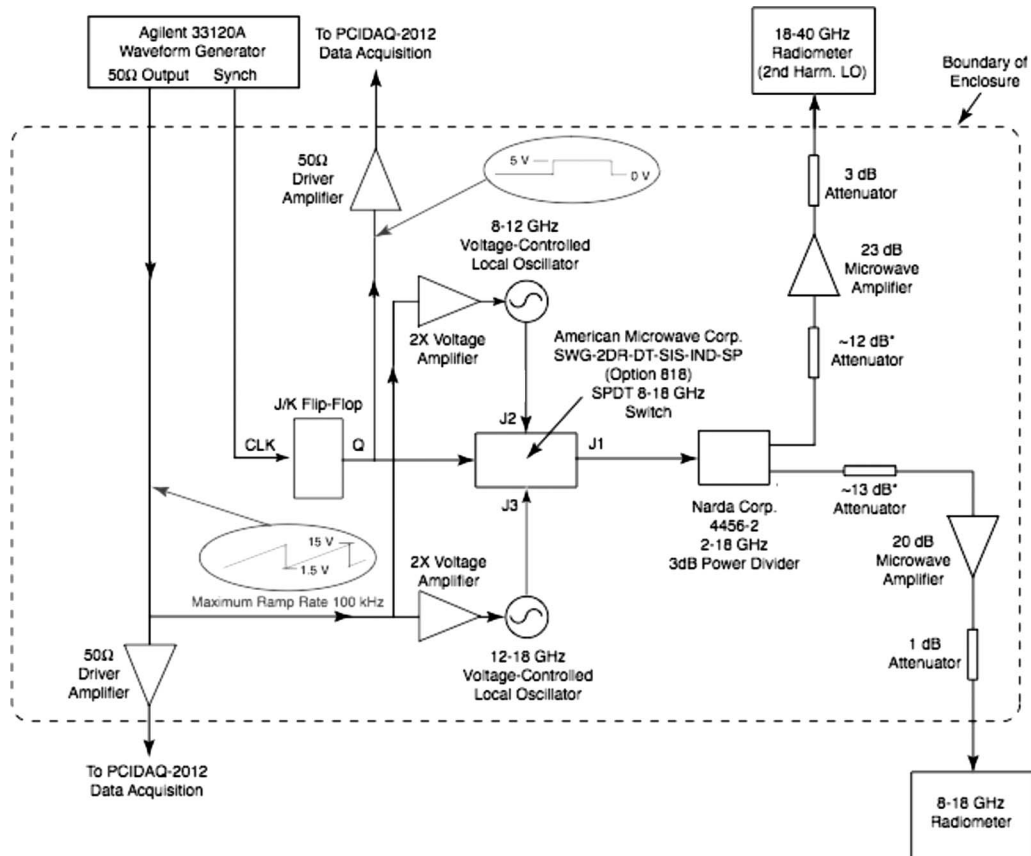
8-18 GHz Switched VCO

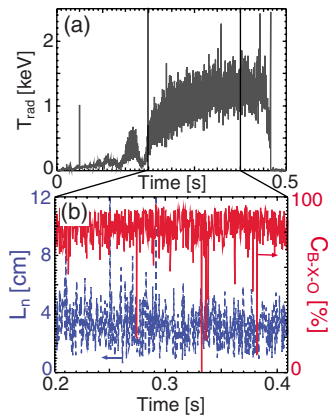FIG. 3. Shown is a schematic of the 8–18 GHz switched VCO system.

FIG. 4. (Color online) (a) The measured 15.5 GHz fundamental emission during a NSTX discharge. (b) The calculated *B-X-O* MC efficiency (solid line), using the measured L_n (dashed line) in Eq. (1a), is shown as a function of time.

sional plasma slab model. A three dimensional ray-tracing code calculates the propagation and absorption of the EBW after MC. The EBE code uses the T_e and n_e profiles measured by laser Thomson scattering[13] and the magnetic equilibrium reconstructed by EFIT.[14] Collisions are incorporated into the EBE code with a Bhatnagar-Gross-Krook collision operator.[15,16]

III. EBE MEASUREMENTS AND SIMULATIONS

A viable EBE $T_e(R,t)$ diagnostic requires the EBW transmission in the plasma and MC to electromagnetic radiation to be efficient, or at least well characterized. EBW research on NSTX has focused on investigating EBE via *B-X-O* coupling to evaluate its use for reconstructing a $T_e(R)$ profile, specifically the effect of density fluctuations (Sec. III A) and EBW collisional damping (Sec. III B) on *B-X-O* transmission efficiency. Being able to quantify these effects allows *B-X-O* coupled thermal EBE to be used for the reconstruction of the $T_e(R)$ profile (Sec. III C).

A. Effects of density fluctuations in T_{rad}

The EBE T_{rad} measurements on NSTX all exhibited a large, up to 90%, fluctuation during both *L*-mode and *H*-mode plasmas, as shown in Fig. 4(a) for fundamental emission from an *L*-mode discharge. The thermal noise fluctuation level for the NSTX EBE diagnostic is calculated to only be ~14%, much lower than the measured fluctuation in T_{rad}. This suggests that the fluctuations in T_{rad} are either due to fluctuations in T_e at the emission location or due to fluctuations in n_e at the MC layer that result in fluctuations in the *B-X-O* MC efficiency. The MC layer for fundamental EBW conversion is typically located within several centimeters of the LCFS. Data from an edge density reflectometer[17] were used to compute L_n at the MC layer for the shot shown in Fig. 4. L_n ranged from 1 to 6 cm during the plasma current flattop [dashed line in Fig. 4(b)]. The measured L_n was inserted into Eq. (1a) to estimate the fluctuation in *B-X-O* MC efficiency. The calculated *B-X-O* MC efficiency for this case ranges from 70% to 90%, agreeing with the measured value of (90 ± 15)%. The measured L_n fluctuation level results in a
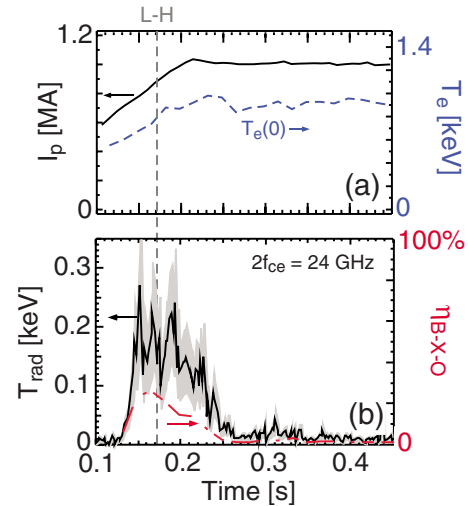

FIG. 5. (Color online) The time evolution of the (a) plasma current, electron temperature and (b) EBE (solid line) and *B-X-O* transmission efficiency (dashed line) for second harmonic emission at 24 GHz. The gray region represents the uncertainty in the EBE measurements.

~25% fluctuation in the *B-X-O* MC efficiency [solid line in Fig. 4(b)]. When reconstructing $T_e(R)$, the maximum value of the measured T_{rad} was used.

B. Effects of EBW collisional damping on EBE

Good *B-X-O* coupling in *H*-mode plasmas is especially important for ST devices that routinely operate in an overdense *H*-mode regime. However, while good fundamental *B-X-O* transmission was measured for *L*-mode plasmas,[18] early EBE measurement in NSTX *H*-mode plasmas revealed very low *B-X-O* transmission efficiencies of only a few percent during the plasma current flattop phase of the discharge. The *B-X-O* transmission efficiency, η_{B-X-O}, accounts for all the EBW losses due to reabsorption, re-emission, and MC the EBW experiences between the point where it is emitted and when it is detected. During initial *B-X-O* emission measurements in *H*-mode plasmas, *B-X-O* transmission efficiencies were 20%–60% for f_{ce}, $2f_{ce}$, and $3f_{ce}$ (18–36 GHz) emission at the *L-H* transition, but decayed to a few percent during the *H*-mode phase [Fig. 5(b)]. Preinhaelter *et al.*[10] first suggested EBW collisional damping[19] as the cause for the observed decay in EBE seen in NSTX *H*-mode plasmas. EBW collisional damping can become important if the local T_e between the emitting EC layer and the MC is less than 30 eV. For these temperatures, the local collision frequency can be high enough that the EBW experiences significant collisional damping, resulting in little or no EBW power being converted to the *X* and *O* modes. For times prior to $t=0.25$ s (for the case shown in Fig. 5), the second harmonic *B-X-O* MC layer is located within 1 cm of the LCFS where $T_e > 20$ eV. For times greater than 0.25 s for this discharge, the MC layer is shifted 3–9 cm outside of the LCFS, where T_e is lower than 10 eV. EBE simulations for 18 GHz fundamental emission of this plasma without incorporating EBW collisional damping prior to MC predict a relatively constant value of $T_{rad} \sim 0.8$ keV, significantly larger than the measured T_{rad} of less than 20 eV. When collisional damping of EBWs prior to MC is included, the simulations reproduce the
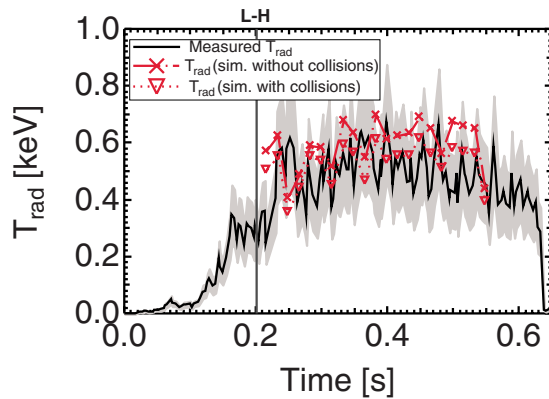
FIG. 6. (Color online) The measured (solid line) and simulated (dashed lines) EBE for fundamental emission during a NSTX H-mode discharge (124306) is shown as a function of time. Little difference is observed between the simulated T_{rad} without collisional effects (dashed line indicated with X's) and with collisional effects (dotted lines indicated with triangles), suggesting EBW collisional damping is significantly reduced. The shaded gray area represents the uncertainty in the EBE measurements.

measured T_{rad} decay during H mode, shown in Fig. 5(b). The EBE simulations predict that the collision frequency near the MC layer increases over a factor of 3 for times greater than $t=0.25$ s and as a result the emission power decreases over a factor of 3. The very low B-X-O transmission efficiencies observed during H-mode plasmas [Fig. 5(b)] make EBE $T_e(R)$ measurement impossible. These results also suggest that if the edge collisionality can be reduced it may be possible to reconstruct a temperature profile from EBE measurements. One method of reducing the edge collisionality is through lithium edge conditioning.

On NSTX lithium evaporation[20] has been used to reduce the density in the plasma scrape off and in the vicinity of the LCFS. For H-mode discharges without lithium conditioning, the MC layer for fundamental EBE was typically located >5 cm outside of the LCFS, where $T_e<10$ eV. A lithium evaporation rate of 19 mg/min was used to reduce n_e by a factor of 2 in the plasma scrape off so that the MC layer was moved to the LCFS, where $T_e>20$ eV. With edge conditioning the emission remained at a constant level throughout the H-mode phase of the discharge (solid line in Fig. 6). For 18 GHz fundamental EBE, the B-X-O transmission efficiency increased from a few percent with no lithium conditioning to 60% with lithium conditioning. Similarly, the B-X-O transmission efficiency for second harmonic emission increased from a few percent to 50% with the addition of lithium edge conditioning. The use of edge conditioning reduced the EBW power lost to collisional damping to only 20%, as compared to 90% without edge conditioning. Good agreement between the measured and simulated T_{rad} with collisions was observed (Fig. 6), allowing the B-X-O transmission efficiency to be calculated for use in reconstructing the $T_e(R)$ profile.

C. T_e reconstruction

To reconstruct the $T_e(R)$ profile using EBE data, the ray-tracing code contained in the EBE simulation code was used to map the emission frequency to an emission radius, $R_{emission}$. The time evolution of the plasma current, central
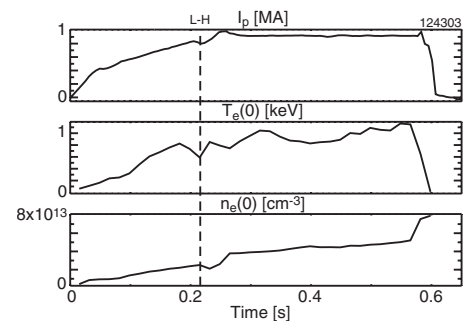

FIG. 7. The time evolution of the (a) plasma current, (b) $T_e(0)$ and (c) $n_e(0)$ are shown for NSTX H-mode discharge 124303.

electron temperature and density for this plasma are shown in Fig. 7. The time of $t=0.365$ s was chosen to reconstruct the T_e profile because it was well into the plasma current flattop when all global parameters had become quasistationary. The emission frequency ranges measured were 18–22 GHz and 26–32 GHz. This frequency range provided T_{rad} measurements from major radius, $R=0.8$–1.45 m; however, the $R_{emission}$ for these frequency ranges was primarily from near the plasma magnetic axis ($R_0=1.0$ m) and the plasma edge ($R>1.4$ m).

The reconstructed $T_e(R)$ from the EBE measurements is shown as a function of major radius in Fig. 8 and is compared to the $T_e(R)$ profile measured by laser Thomson scattering. T_e is reconstructed from the measured T_{rad} by dividing the measured T_{rad} by the simulated B-X-O transmission efficiency, η_{B-X-O}. The simulated B-X-O transmission efficiency accounts for all of the losses due to re-absorption and re-emission, as well as losses due to EBW collisional damping prior to MC. The emission radius was taken to be a weighted average of the emission radius for the 41 rays used to simulate the antenna beam waist in the EBE simulation. The radial error bars in Fig. 8 represent one weighted standard deviation of the emission location for the 41 rays. The vertical error bars represent the uncertainty in the T_{rad} measurement. Highly localized emission is seen for emission locations in the region $R>1.41$ m. The large radial spread for T_{rad} from $R<1.4$ m can be attributed to emission simultaneously coming from the fundamental and second harmonics, so that the emission location varied between 0.8 and 1.5 m for the 41 rays (Fig. 9). Good agreement is observed between T_{rad} and the Thomson scattering edge profile for R
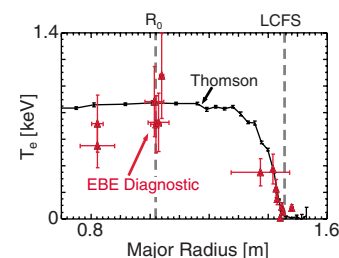

FIG. 8. (Color online) The EBE measured $T_e(R)$ ($=T_{rad}/\eta_{B-X-O}$) is indicated by the triangles and plotted as a function of major radius for the discharge shown in Fig. 7 at $t=0.365$ s. The radial error bars represent the weighted emission location using 41 rays to simulate the beam waist. The vertical error bars represent the uncertainty in the EBE measurements. The solid line shows the T_e profile from Thomson scattering at $t=0.365$ s.
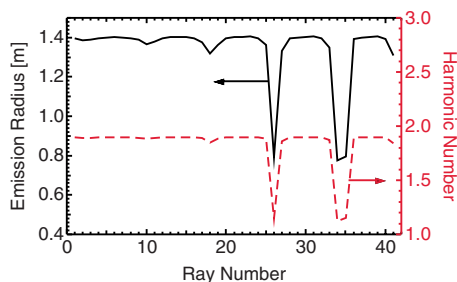
FIG. 9. (Color online) The emission location (solid black) and the harmonic number (dot dashed) are shown for the 41 rays used in the EBE simulation for 19.5 GHz emission. This frequency had the largest radial extent due to the contributions from fundamental and second harmonic emission locations. The noninteger harmonic numbers indicate the emission originates from a Doppler-broadened resonance location.

> 1.4 m. EBWs emitted from the plasma edge have much less plasma to propagate through; therefore, there is less power loss of the EBW due to reabsorption and re-emission. In addition, there is less harmonic overlap for edge emission (as seen in Fig. 10), so the emission is much more highly localized. All of the emission from the plasma edge comes from a region no more than 2 cm in radial width (Fig. 11). The radial extent of the core emission is anywhere from 2 to 15 cm, as indicated by the radial bars in Fig. 8 and shown in detail for 28 GHz emission in Fig. 11.

IV. DISCUSSION

Measuring the $T_e(R)$ profile via *B-X-O* emission measurements in the ST is difficult. The *B-X-O* process is complicated, involving double MC of the emission before it is detected, and an antenna view oblique to the magnetic field near the plasma edge, so that extensive numerical modeling is needed to determine the emission location and hence reconstruct the $T_e(R)$ profile. In contrast to stellarators or conventional aspect ratio tokamaks, reconstruction of the magnetic equilibrium in a ST is strongly affected by time varying internal currents that generate poloidal fields that can be comparable to the toroidal field. In addition, significant Doppler broadening can lead to reabsorption and re-emission of the radiation as it travels through the plasma. Although the EBE simulation code provides a method to calculate these losses and determine the emission location used for $T_e(R)$ reconstructions, the code results are very sensitive to the reconstructed magnetic equilibrium from EFIT and the T_e and
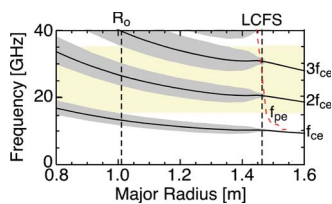

FIG. 10. (Color online) The characteristic frequency plot is shown for *H*-mode discharge 124303. The first three EC harmonics (solid lines) and *O*-mode cutoff (dashed line) are shown as a function of major radius. The gray regions surrounding the EC harmonics indicate the Doppler shifted resonance frequency. The light shaded box indicates the frequency range of the radiometer system.
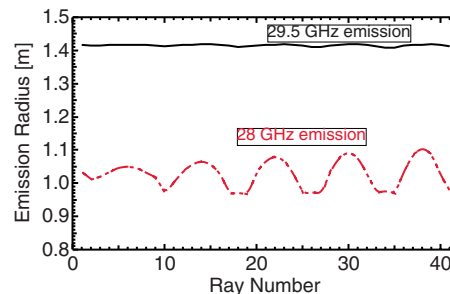

FIG. 11. (Color online) The emission location for the 41 rays used in the EBE simulation code to model the antenna beam waist is shown for 28 GHz (dot dashed) and 29.5 GHz (black solid) emission.

n_e profiles from Thomson scattering. An accurate description of the antenna pattern of the EBE diagnostic and its orientation is also required for accurate EBE simulations. If any of these input data is inaccurate, the emission location of the EBWs will not be correctly calculated, and the $T_e(R)$ profile will be poorly reconstructed. In addition, density fluctuations at the *B-X-O* MC layer lead to large fluctuations in the *B-X-O* transmission efficiency and EBW collisional damping can significantly reduce the *B-X-O* transmission efficiency or sometimes entirely absorb the EBW before MC occurs. Lithium edge conditioning has been used successfully to mitigate the EBW collisional damping and as a result increase EBW coupling efficiency to 60%.

[1] M. R. Bornatici, R. Cano, O. De Barbiere, and F. Englemann, Nucl. Fusion **23**, 1153 (1983).
[2] M. Ono *et al.*, Nucl. Fusion **40**, 557 (2000).
[3] I. B. Bernstein, Phys. Rev. **109**, 10 (1958).
[4] A. K. Ram and S. D. Schultz, Phys. Plasmas **7**, 4084 (2000).
[5] J. Preinhaelter and V. Kopecky, J. Plasma Phys. **10**, 1 (1973).
[6] E. Mjølhus, J. Plasma Phys. **31**, 7 (1984).
[7] F. R. Hansen, J. P. Lynoc, C. Maroli, and V. Petrillo, J. Plasma Phys. **39**, 319 (1988).
[8] S. J. Diem *et al.*, Rev. Sci. Instrum. **77**, 10E919 (2006).
[9] R. H. Dicke, Rev. Sci. Instrum. **17**, 268 (1946).
[10] J. Preinhaelter, J. Urban, P. Pavlo, G. Taylor, S. Diem, L. Vahala, and G. Vahala, Rev. Sci. Instrum. **77**, 10F524 (2006).
[11] A. K. Ram, A. Bers, and C. N. Lashmore, Phys. Plasmas **9**, 409 (2002).
[12] J. Urban and J. Preinhaelter, J. Plasma Phys. **72**, 1041 (2006).
[13] B. P. LeBlanc, R. E. Bell, D. W. Johnson, D. E. Hoffman, D. C. Long, and R. W. Palladino, Rev. Sci. Instrum. **74**, 1659 (2003).
[14] L. Lao, H. St. John, R. D. Stambaugh, A. G. Kellman, and W. Pfeiffer, Nucl. Fusion **25**, 1611 (1985).
[15] P. L. Bhatnagar, E. P. Gross, and M. Krook, Phys. Rev. **94**, 511 (1954).
[16] E. P. Gross and M. Krook, Phys. Rev. **102**, 593 (1956).
[17] J. B. Wilgen, G. R. Hanson, T. S. Bigelow, D. W. Swain, P. M. Ryan, M. D. Carter, J. R. Wilson, and the NSTX Team, APS-DPP Conference Proceedings, Long Beach, CA, 2001 (unpublished).
[18] G. Taylor *et al.*, Phys. Plasmas **12**, 052511 (2005).
[19] S. Pesic, Physica C **125**, 118 (1984).
[20] H. W. Kugel *et al.*, J. Nucl. Mater. **363–365**, 791 (2007).